Published OnlineFirst December 27, 2017; DOI: 10.1158/1535-7163.MCT-17-0813

Large Molecule Therapeutics

Molecular Cancer Therapeutics

An Anti-GDNF Family Receptor Alpha 1 (GFRA1) Antibody–Drug Conjugate for the Treatment of Hormone Receptor–Positive Breast Cancer

Sunil Bhakta, Lisa M. Crocker, Yvonne Chen, Meredith Hazen, Melissa M. Schutten, Dongwei Li, Coenraad Kuijl, Rachana Ohri, Fiona Zhong, Kirsten A. Poon, Mary Ann T. Go, Eric Cheng, Robert Piskol, Ron Firestein, Aimee Fourie-O'Donohue, Katherine R. Kozak, Helga Raab, Jo-Anne Hongo, Deepak Sampath, Mark S. Dennis, Richard H. Scheller, Paul Polakis, and Jagath R. Junutula

Abstract

Luminal A (hormone receptor-positive) breast cancer constitutes 70% of total breast cancer patients. In an attempt to develop a targeted therapeutic for this cancer indication, we have identified and characterized Glial cell line–Derived Neurotrophic Factor (GDNF) Family Receptor Alpha 1 (GFRA1) antibody–drug conjugates (ADC) using a cleavable valine-citrulline-MMAE (vcMMAE) linker-payload. RNAseq and IHC analysis confirmed the abundant expression of GFRA1 in luminal A breast cancer tissues, whereas minimal or no expression was observed in most normal tissues. Anti–GFRA-vcMMAE ADC internalized to the lysosomes and exhibited target-dependent killing of GFRA1-expressing cells both *in vitro* and *in vivo*. The ADCs using humanized anti-GFRA1 antibodies displayed robust therapeutic activity in clinically relevant cell line–derived (MCF7 and KPL-1) tumor xenograft models. The lead anti-GFRA1 ADC cross-reacts with rodent and cynomolgus monkey GFRA1 antigen and showed optimal pharmacokinetic properties in both species. These properties subsequently enabled a target-dependent toxicity study in rats. Anti-GFRA1 ADC is well tolerated in rats, as seen with other vcMMAE linker–payload based ADCs. Overall, these data suggest that anti–GFRA1-vcMMAE ADC may provide a targeted therapeutic opportunity for luminal A breast cancer patients. *Mol Cancer Ther; 17(3); 638–49. ©2017 AACR.*

Introduction

Breast cancer is the most frequently diagnosed cancer in women. In the year 2016, there were 246,660 women estimated to be diagnosed with breast cancer and over 40,450 reported deaths in the United States (1). Breast cancer can be further classified into four molecular subtypes based on the presence or absence of hormone (estrogen or progesterone) receptors (HR^+/HR^-) and excess levels of human epidermal growth factor receptor 2 ($HER2^+/HER2^-$): Luminal A ($HR^+/HER2^-$), Luminal B ($HR^+/HER2^+$), $HER2^-$ enriched ($HR^-/HER2^+$), and triple-negative ($HR^-/HER2^-$; ref. 2). Luminal A, a slow growing, less aggressive cancer among the four subtypes, represent 74% of total breast cancer cases. In addition to hormone therapy, there are several targeted therapeutic treatment options that can either inhibit the hormone receptor signaling or lower hormone receptors levels. The HER2-enriched subgroup representing 4% of all breast cancers, is the most aggressive cancer, but with several HER2-targeted treatment options (3). Luminal B constitutes 10% of cases and can either be treated using luminal A cancer treatment options or available HER2-targeted therapies. Triple-negative breast cancer, comprising 12% of total cases, currently has no approved targeted therapies (2).

The most common and effective treatment for luminal A breast cancer is endocrine therapy, which targets the function of the estrogen receptor (ER) by using ER modulators (e.g., tamoxifen), ER downregulators (e.g., fulvestrant) or by blocking estrogen biosynthesis (e.g., aromatase inhibitors; ref. 4). There is still a major unmet need to develop targeted therapies to treat luminal A breast cancer patients due to the development of resistance for the current treatment options. For example, *de novo* or acquired resistance to aromatase inhibitor therapy limits their benefit for many breast cancer patients. Glial cell line–Derived Neurotrophic Factor (GDNF)-RET signaling was shown to be a key determinant of resistance to aromatase inhibitor therapy in ER^+ breast cancer patients (4). In addition, both RET and GFRA1 proteins, key cell-surface receptors for GDNF signaling, were shown to be overexpressed in ER^+ breast cancer (5). Developing targeted therapies

Genentech, Inc., 1 DNA Way, South San Francisco, California.

Note: Supplementary data for this article are available at Molecular Cancer Therapeutics Online (http://mct.aacrjournals.org/).

Corrected online October 22, 2019.

Current Address for C. Kuijl: VU Medical Center, Amsterdam, the Netherlands; current address for R. Firestein, Hudson Institute of Medical Research, Monash University, Clayton, VIC 3168, Australia; current address for J.-A. Hongo, JS Hongo Consulting, Inc., 855 Jefferson Avenue 1204, Redwood City, California; current address for M.S. Dennis, Denali Therapeutics, Inc., 151 Oyster Point Boulevard, South San Francisco, California; current address for R.H. Scheller, 23andMe, Inc., 349 Oyster Point Boulevard, South San Francisco, California; and current address for J.R. Junutula, Cellerant Therapeutics, Inc., 1561 Industrial Road, San Carlos, California.

Corresponding Authors: Sunil Bhakta, Genentech, Inc., 1 DNA Way, South San Francisco, California, 94080. Phone: 650-467-3695; Fax: 650-225-1411; E-mail: sbhakta@gene.com; and Jagath R. Junutula, jagathjr@gmail.com

doi: 10.1158/1535-7163.MCT-17-0813

Published OnlineFirst December 27, 2017; DOI: 10.1158/1535-7163.MCT-17-0813

similar to Kadcyla, a HER2-targeting antibody–drug conjugate (ADC) for $HER2^+$ breast cancer, could therefore be an attractive option for the unmet need in treating luminal A breast cancer patients. ADCs have been undergoing intensive investigation in the preclinical as well as clinical setting for the past 30 years and there are currently over 60 ADCs currently in clinical trials (6, 7).

In this article, we have identified GFRA1 as a luminal A (hormone receptor- positive) breast cancer target and have developed a humanized anti-GFRA1 ADC that demonstrates specific *in vitro* and *in vivo* killing of GFRA1-expressing cells. In addition, the ADC displays therapeutic features, including a target safety profile and pharmacokinetic (PK) properties that would enable its progress toward further development into the clinic.

Materials and Methods

Cell lines

All cell lines used in this article were from Genentech cell culture facility (gCell) that originally obtained them either from the ATCC or NCI-60 (National Cancer Institute). Identity of all cell lines was confirmed by DNA testing (STR profiling) and they lacked mycoplasma contamination. MCF7-neo/HER2 cell line was established at Genentech, Inc. All cells were grown in appropriate media at 37°C with 5% CO_2.

Plasmid constructs and transfections

The full-length GFRA1 clone was initially obtained from Invitrogen Life Technology and subsequently PCR amplified for subcloning into the pRKneo vector (Genentech). Transfections were performed using FuGENE 6 (Roche Applied Science), and an empty vector was used as control.

Processing and expression analysis of TCGA RNAseq data

RNAseq reads were first aligned to ribosomal RNA sequences to remove ribosomal reads. The remaining reads were aligned to the human reference genome (NCBI Build 38) using GSNAP version "2013-10-10," allowing a maximum of two mismatches per 75 base sequence (parameters: "-M 2 -n 10 -B 2 -i 1 -N 1 -w 200000 -E 1 –pairmax-rna=200000 – clip-overlap"; ref. 8). Transcript annotation was based on the RefSeq database (NCBI Annotation Release 106.). To quantify gene expression levels, the number of reads mapped to the exons of each RefSeq gene was calculated. Read counts were normalized by library size and precision weights calculated using the voom R package (9). Subsequently, differential expression analysis on the normalized count data was performed using the limma R package (10). Gene expression is displayed in form of normalized Reads Per Kilobase gene model per Million total reads (nRPKM) as described in Srinivasan and colleagues (11).

Preparation of total RNA and real-time PCR

Frozen breast cancer tissues were obtained from Genentech tissue bank. Total RNA was prepared from 10 to 20 mg of tissue using the RNeasy Mini (Qiagen) Kit as per the manufacturer's protocol. For assessing RNA quality and yield, A260/A280 and A260/A230 ratios for RNA preparation samples were analyzed with a Nano-Drop ND-1000 spectrophotometer (NanoDrop Technologies). RNA integrity was determined by 28S/18S rRNA visualization in agarose gel, stained with ethidium bromide and they were then stored at −80°C for later use. GFRA1 and RET expression levels were measured using custom-made TaqMan primer/probe spanning across exon junctions. The TaqMan probes were labeled with FAM as reporter dye and TAMRA as quencher dye (Fwd: 5′-TCGACGACATTTGCAAGAAGTAC -3′; Rev: 5′-GGCGGTTGCAGACATCATT-3′; FAM probe, 5′-CGTACATCACCCCGTGCACCACC-3′). Samples were prepared as per the manufacturer's protocol using TaqMan RNA- to- CT 1-step kit (Applied Biosystems, catalog no.4392938). Samples were analyzed using ABI Prism7500 Real-Time detection instrument. Samples were normalized to a housekeeping gene (RPL19). The data output is expressed as a fold-difference comparing with normal breast tissue (control).

Development and characterization of mouse anti-GFRA1 antibodies

Balb/c mice (Charles River Laboratories) were immunized in the footpads twice weekly with 4 μg human GFRA1 protein fused to a human Fc (R&D Systems) mixed with MPL+TDM adjuvant. Popliteal lymph nodes were harvested three days after the last immunization. Lymphocytes from these mice, all of whose sera demonstrated strong binding to the immunizing protein, as well as strong binding to 293 cells overexpressing GFRA1 by FACS, were fused with X63-Ag8.653 mouse myeloma cells (ATCC) via electrofusion (Cytopulse) and incubated at 37°C, 7% CO_2, overnight in DMEM (Lonza) supplemented with 10% FBS, 4.5 g/L glucose, 25 mmol/L HEPES, 0.15 mg/mL oxaloacetic acid, 100 μg/mL pyruvic acid, 0.2 U/mL Insulin, 2 mmol/L L-glutamine, 100 U/mL penicillin, 100 μg/mL streptomycin (Penicillin-Streptomycin, Invitrogen), NCTC-109 (Lonza), non-essential amino acids (Invitrogen), before plating into 96-well plates supplemented with 5.7 μmol/L azaserine and 100 μmol/L hypoxanthine (HA, Sigma-Aldrich). Cells were cultured for 10 days, followed by ELISA and FACS analyses. Cells from wells demonstrating expression of mouse IgG and showing strong specific binding by ELISA and FACS were expanded and subcloned by limiting dilution. Final clones demonstrating the highest FACS binding or specific staining by IHC after the second round of subcloning was expanded for large-scale production in bioreactors (Integra Biosciences). Supernatants were purified by liquid chromatography using a Protein A column.

Preparation of small-scale (<1 mg) anti-GFRA1 ADCs using a high-throughput–based 96-well format

Each anti-GFRA1 antibody was conjugated to the maleimide-based thiol-reactive vcMMAE (maleimidocaproy-valine-citrulline-p-aminobenzoyloxycarbonyl MMAE) linker-payload (12) in separate reactions. A high-throughput–based on-bead Protein A conjugation and purification method was developed using a 96-well plate format. Complete reduction of the endogenous cysteines, followed by conjugating with 2:2:1 ratio of vcMMAE:N-ethyl maleimide:Alexa488-maleimide was used to obtain a drug to antibody ratio (DAR) of 3.5 per mAb and 1–2 Alexa488 fluorophores per mAb. This resulted in a dual-labeled antibody conjugate with both vcMMAE and Alexa488. The concentration of all small-scale ADCs was determined and normalized using the ratio of UV280 and Alexa488 fluorescence.

Humanization of murine anti-GFRA1 antibodies

Site-directed mutagenesis was used to graft the hyper-variable regions from murine anti-GFRA1 antibodies, mu-6D3 and mu-7C9 into human framework. Briefly, mu-6D3 and mu-7C9 were aligned to the closest human consensus framework, namely

Published OnlineFirst December 27, 2017; DOI: 10.1158/1535-7163.MCT-17-0813

kappa subgroup II for the VL domain and subgroup III for the VH domain. Key Vernier/framework residues were tested to evaluate their contributions for maintaining parental affinity in the initial set of graft variants. Fabs of the CDR graft variants were made and affinity determined by using surface plasmon resonance (SPR) on a Biacore instrument (GE Healthcare Life sciences). Humanized versions of mu-6D3 and mu-7C9 (hu-6D3 and hu-7C9) had similar affinity to that of their murine counterparts. However, there was a cysteine in VH-CDR1 VH35 in the original mu-6D3 antibody which was anticipated to be problematic for maintaining binding affinity, so a few conservative substitutions at VH35, namely VH C35A, VH C35T, and VH C35S were investigated. Biacore experiments demonstrated that all these conservative single substitutions resulted in approximately 5-fold lower affinity as compared to original. Subsequently, affinity maturation was carried out on C35S variant as described earlier (13, 14). We have successfully identified an affinity-matured variant (hu-6D3.v5) that was shown to be equivalent to the parental clone (hu-6D3) by Biacore. Final humanized variants were named as hu-6D3.v5 and hu-7C9.

Purification of antibodies and preparation of large scale ADCs

Chimeric and humanized IgG1 antibodies described in this manuscript were transiently expressed in CHO cells and purified using standard Protein-A and ion-exchange chromatography methods. All antibodies were conjugated with vcMMAE as described previously (12). DAR for all ADCs was determined by LC/MS. The concentration and aggregation status of each ADC were determined using automated liquid chromatography methods.

Fluorescence microscopy

HEK293T cells were seeded in Lab-Tek II cell culture-treated 4-well chamber slides (Nalge Nunc International) and incubated with 2 μg/mL Alexa488 conjugated GFRA1 mAb (ch-6D3) in the presence of the lysosomal protease inhibitors leupeptin and pepstatin A (Sigma-Aldrich) at 50 and 5 nmol/L, respectively, and incubated for 60 minutes on ice and then continued the incubation for either 0, 2, 4, and 16 h in a 37°C incubator with 5% CO_2. Cells were then washed with PBS and fixed in 4% paraformaldehyde (Polysciences, Inc.) for 5 minutes at room temperature and permeabilized with 0.1% TX-100 in PBS with 0.5% BSA for 5 minutes at 37°C. Cells were then incubated for 1 hour with 2 μg/mL mouse anti-LAMP2 (BD Biosciences, cat# 555803) followed by 1 hour incubation of Alexa647-labeled rabbit anti-mouse IgG (Jackson ImmunoResearch Laboratories, Inc., cat# 715-605-151).

IHC

IHC was performed on 4-μm-thick formalin-fixed, paraffin-embedded tissue sections mounted on glass slides. All IHC steps were carried out on the Ventana Discovery XT (Ventana Medical Systems) autostainer. Pretreatment was done with cell conditioner 1, standard time. Primary antibody goat anti-GFRA1 polyclonal antibodies (R&D Systems, Inc., catalog no. AF714) were used at a concentration of 10 μg/mL and were incubated on slides for 1 hour at 37°C. Ventana Mouse OmniMap (Ventana Medical Systems) was used as the detection system. Ventana DAB and hematoxylin II were used for chromogenic detection and counterstain. IHC scoring was done using following criteria: negative: no detectable signal in >50% of tumor cells, 1+ score: positive signal in >50% of tumor cells with majority of weak signal; 2+ score: positive signal in >50% of tumor cells with majority of moderate signal; 3+ score: positive signal in >50% of tumor cells with majority of strong signal.

Western blot analysis

Whole-cell lysates were prepared from cancer cell lines, and standard Western blot analysis was performed. Proteins were resolved by 4%–12%Tris SDS-PAGE, and analyzed by Western blotting using Pathscan Multiplex Western Cocktail (Cell Signaling Technology). Membranes were then incubated with horseradish peroxidase (HRP)–conjugated goat anti-mouse IgG (Bio-Rad) or goat anti-rabbit IgG (Cell Signaling Technology) followed by ECL detection. Phospho-MAPK (p44/42) and Erk1/Erk2 were detected using anti-p44/42 MAPK antibody (Cell Signaling Technology, catalog no. 5301) and anti-Erk1/Erk2 antibody (Cell Signaling Technology, catalog no. 5301), anti-Rab11 (Cell Signaling Technology, catalog no. 5301), and anti-Phospho S6 antibody (Cell Signaling Technology, catalog no. 5301) were used to detect Rab11 and phosphorylated form of S6 proteins, respectively.

In vitro cell proliferation

Proliferation in the presence of ADCs was assessed using cells plated at 2,000/well in 50 μL of normal growth medium in 96-well clear-bottom plates (PerkinElmer Life Sciences). Twenty-four hours later, an additional 50 μL of culture medium with serial dilutions of ADCs were added in triplicate. Three or 5 days later, cell numbers were determined using CellTiter-Glo (Promega) and with an EnVision 2101 multilabel reader (PerkinElmer).

Mouse xenograft efficacy studies

All *in vivo* efficacy studies were approved by Genentech's Institutional Animal Care and Use Committee (IACUC) and adhere to the NIH Guidelines for the Care and Use of Laboratory Animals. Naïve female NCr nude or C.B-17 SCID beige mice (Taconic or Charles River Laboratories) were inoculated in the #2/3 mammary fat pad with 5 million KPL-1 or MCF7-neo/HER2 cells suspended in HBSS and Matrigel (BD Biosciences). Naïve female NCr nu/nu mice (Charles River Laboratories) were inoculated subcutaneously with 10 million MCF7 cells suspended in HBSS. One to 4 days before inoculation of the MCF7 or MCF7-neo/HER2 cells, mice were implanted subcutaneously with a 0.36 mg, 60-day sustained release 17β estradiol pellet (Innovative Research of America). Once tumors reached a mean volume of 195–350 mm^3, mice with similarly sized tumors were randomized into treatment groups ($n = 8$–10/group) and an intravenous dose of vehicle (20 mmol/L Histidine- Acetate Buffer), mu control ADC (mu-gp120-ADC), mu-anti-GFRA1 ADCs, hu-control ADC (hu-gD-ADC), or hu-anti–GFRA1 ADCs were administered. Length (l) and width (w) of each tumor were measured using digital calipers (Fred V. Fowler Company, Inc.) and tumor volumes were calculated ($V = lw^2 \times 0.5$). A linear mixed modeling approach was used to analyze the repeated measurement of tumor volumes from the same animals over time. Curve fitting was applied to $\log_2$-transformed individual tumor volume data using a linear mixed-effects (LME) model with the R package nlme, version 3.1–97 in R v2.13.0 (R Development Core Team 2008; R Foundation for Statistical Computing). Partial response (PR) is defined as a tumor regression of >50% but <100% of the starting tumor volume, and complete response (CR) is defined as 100%

Published OnlineFirst December 27, 2017; DOI: 10.1158/1535-7163.MCT-17-0813

tumor regression (i.e., no measurable tumor) on any day during the study. These values are calculated on an individual animal basis from the raw data. In all studies, tumor volumes and body weights were collected at least once weekly for the duration of the study. Mice with tumor volumes $\geq$2,000 mm^3 or with losses in body weight $\geq$ 20% from their weight at the start of treatment were euthanized per IACUC guidelines. The sparse pharmacokinetic samples were taken at days 1, 7, and 14 postdose in KPL-1 or MCF7-neo/HER2 xenograft studies.

Pharmacokinetic studies in Sprague Dawley rats and cynomolgus monkeys

The pharmacokinetic study in female Sprague Dawley rats was approved by the IACUC at Genentech, Inc. Rats received a single intravenous dose of either hu-6D3.v5 or hu-7C9 at 0.5 or 5 mg/kg via the jugular vein cannula ($n = 4$/group). Serial serum samples were collected from the tail vein and the terminal blood sample was collected via cardiac stick from each animal in each dosing group at the following time points: 10 minutes; 1, 6, and 24 hours; and 2, 3, 7, 10, 14, 21, and 28 days post dose. Serum concentration–time data were used to estimate relevant pharmacokinetic parameters.

Sixteen naïve male cynomolgus monkeys of Chinese origin were obtained by Covance Research Products Inc. Animals were 2- to 4-year-old and assigned to four groups (4 animals/group) by a stratified randomization scheme designed to achieve similar group mean body weights. Monkeys received a single intravenous bolus injection of either hu-6D3.v5 or hu-7C9 at 0.3 or 3 mg/kg. Blood samples for pharmacokinetic analysis were collected postdose at 0.25, 4, and 12 hours and on days 1, 3, 4, 7, 10, 14, 21, 28, 35, and 42. Serum concentration–time data were used to estimate relevant pharmacokinetic parameters.

Bioanalysis of serum and plasma samples from pharmacokinetic studies

Serum concentrations of two antibodies, hu-6D3.v5 and hu-7C9, following an intravenous administration in rats and cynomolgus monkeys, or total antibody (tAb, both conjugated and unconjugated antibodies) following an intravenous administration of ADC in mice, were analyzed by a generic total antibody semihomogeneous immunoassay. This assay consisted of NeutrAvidin (Pierce) coated onto NUNC Maxisorp plates to capture biotinylated sheep anti-human IgG (Binding Site) bridged with conjugated or unconjugated antibody, and goat anti-human IgG-HRP (Bethyl Laboratories Inc.) as the detection reagent. Bound HRP–antibody conjugate was measured with a solution of tetramethylbenzidine/H_2O_2. The plate was read for absorbance at 450 nm with a reference wavelength of 650 nm. The concentration was determined with the 4-p fit curve using Prism 6. The minimum reportable value for this assay was 16.4 ng/mL.

Mouse serum concentrations of conjugated antibody were characterized by an ELISA. The assay used an anti-MMAE monoclonal antibody (SG 3.247) as the capture reagent and goat anti-human IgG (Bethyl Laboratories Inc.) conjugated to HRP for detection. The minimum reportable value was 16.4 ng/mL in serum.

Pharmacokinetic data analysis

The serum concentration versus time data from each animal following an intravenous administration was analyzed using intravenous bolus input model (Model 201; WinNonlin, Pharsight Corporation). The following noncompartmental estimation of pharmacokinetic parameters were reported: observed maximum serum concentration (C_{max}), total drug exposure defined as area under the serum concentration–time curve extrapolated to infinity (AUC_{inf}); Clearance (Dose/AUC_{inf}), half-life of the elimination phase ($t_{1/2}$), and volume of distribution at steady state (Vss). Each animal was analyzed separately and results for each dose group were summarized as mean $\pm$ SD.

Rat toxicology study

To investigate the toxicity and tolerability of anti–GFRA1-vc-MMAE ADC, a repeat dose study was conducted in Sprague Dawley rats. Rats were dosed intravenously on days 1 and 8 with vehicle alone, or 10 or 20 mg/kg anti–GFRA1-vcMMAE ADC (GFRA1 ADC) or 20 mg/kg nonbinding trastuzumab-vcMMAE ADC (HER2 ADC; $n = 6$ female animals/group). Assessment of toxicity was based on mortality, clinical signs, food consumption, functional observation battery (FOB), motor activity, and clinical and anatomic pathology. Motor activity and FOB were performed during the predose phase and on study day 14. Motor activity evaluation included basic movement, x + y ambulation, fine movements, and rearing activity. FOB examinations included hand-held observations, open-field observations, and elicited behaviors (sensory reactivity to stimuli). Blood collections for hematology and clinical chemistry were collected in all animals on days 5 and 15. Necropsies were performed on day 15 and tissues were routinely processed for histologic examinations, including expanded neurohistopathology of central and peripheral nervous system tissues.

Results

GFRA1 is highly expressed in luminal A breast cancer

Given previous reports of upregulation of GFRA1 and RET in ER^+ breast cancers, we assessed their suitability as ADC target antigens for luminal A breast cancers using expression from The Cancer Genome Atlas (TCGA). We observed a significant upregulation of both GFRA1 and RET in the luminal A and luminal B subtypes over their expression in normal samples (log_2 fold-change of 3.29 and 3.46, with $P < 10^{-4}$, respectively; Fig. 1A and B). In contrast, basal-like tumors displayed significantly reduced GFRA1 expression compared with normal samples (log_2 fold change: -2.55, $P = 7.33 \times 10^{-14}$). To further validate overexpression of GFRA1 and RET in breast cancer tissues, we collected 28 breast cancer tissues, isolated RNA and performed PCR (TaqMan) analysis to quantitate mRNA levels of GFRA1. It is evident from Fig. 1C that GFRA1 is overexpressed in most luminal A breast cancer tissues and also in $HER2^+$ and basal breast cancer tissues, albeit less frequently. In addition, these analyses confirmed that relative expression of GFRA1 is more abundant than RET, thus GFRA1 may be a superior ADC target. Therefore, we went on to further characterize GFRA1 for its use as a target for an ADC therapeutic.

We have validated the use of anti-GFRA1 polyclonal antibodies to conduct IHC analysis on GFRA1 +ve and −ve cell lines as well as breast cancer tumor tissues (Supplementary Fig. S1 and Fig. 1C and D). IHC analysis, using goat anti-GFRA1 polyclonal antibodies further confirmed the RNA-based analysis, TaqMan and IHC analyses are well correlated (Fig. 1D). GFRA1 transcript and protein were not detectable in tumor

Published OnlineFirst December 27, 2017; DOI: 10.1158/1535-7163.MCT-17-0813

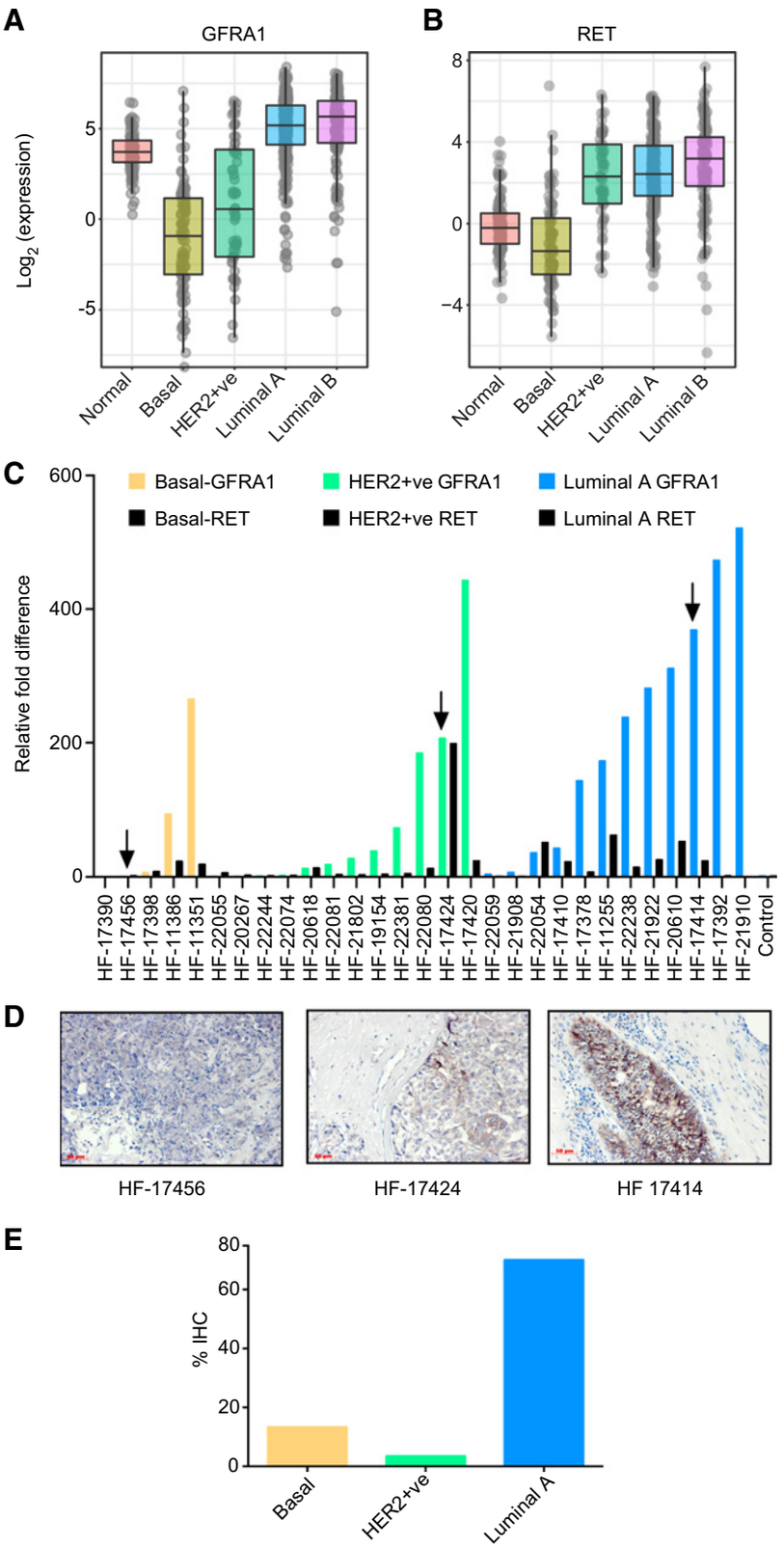

Figure 1.

GFRA1 is overexpressed in luminal A (hormone receptor–positive) breast cancer. Expression of GFRA1 (**A**) and RET (**B**) in TCGA breast cancer RNA-seq data (quantified as $\log_2$ nRPKM), stratified by PAM50 breast cancer subtype. Normal samples were taken from all TCGA indications. **C,** Quantification of GFRA1 and RET transcripts by TaqMan analysis from RNA isolated from breast cancer tissues. **D,** Overexpression of GFRA1 protein as confirmed by Immunohistochemistry (IHC) analysis. Patient samples with arrows in Fig. 2A correspond to the IHC images shown in the Fig. 2B from the same patients. **E,** Percentage of GFRA1-positive ($\geq$IHC 1+) breast tumors in basal ($n = 45$), $HER2^+$ ($n = 28$), and luminal A ($n = 40$) specimens.

Published OnlineFirst December 27, 2017; DOI: 10.1158/1535-7163.MCT-17-0813

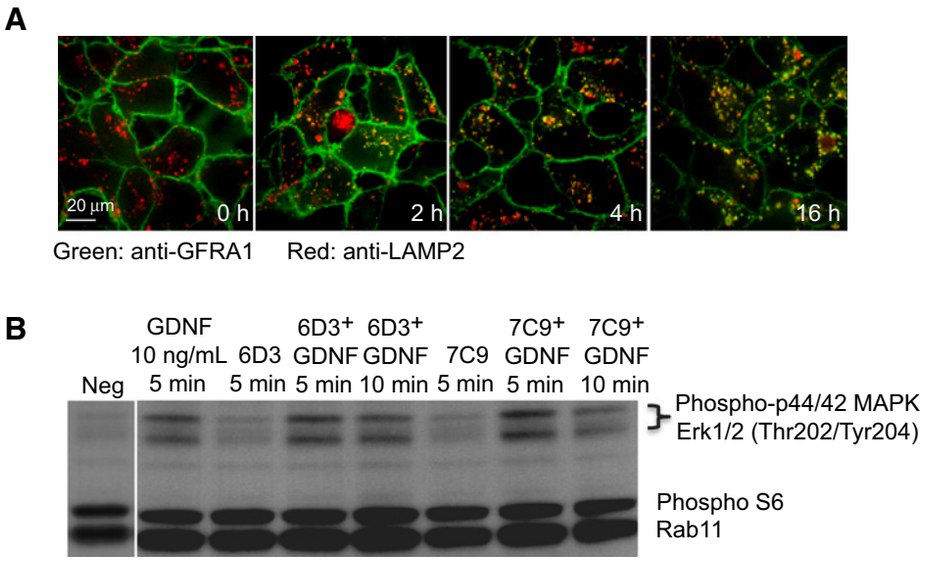

Figure 2.

Development and characterization of anti-GFRA1 antibodies. **A,** Internalization of anti-GFRA1 antibody (6D3). HEK293-overexpressing human GFRA1 were incubated with 2,000 ng/mL 6D3-Alexa488 (green) antibody conjugate for 60 minutes on ice, further incubated at 37°C for various time points and then fixed and co-stained with mouse anti-LAMP2 and Alexa647-labeled rabbit anti-mouse antibodies (red). Merged confocal images are shown in the figure. **B,** Anti-GFRA1 antibodies do not interfere with GDNF induced GFRA1/c-RET signaling. MCF7 cells were pre-incubated for 1 hour with 1,000 ng/mL anti- GFRA1 antibodies (mu-6D3 and mu-7C9) and GDNF/GFRA1/c-RET signaling was induced by addition of GDNF (10 ng/mL) at various time intervals. Cells were harvested and analyzed by Western blotting for phospho MAP Kinase and Erk1/2. Phospho S6 and Rab11 are loading controls.

tissue HF-17456, while moderate and high-expression levels of GFRA1 were seen in HF-17424 (IHC 2+) and HF-17414 (IHC3+), respectively. A total of 113 breast tumor tissues were screened for GFRA1 protein expression by IHC analysis and 70% (28 out of 40) of luminal A samples showed strong GFRA1 expression (IHC 2+/3+), whereas only 6 out 45 (13%) basal breast cancer and 1 out of 28 $HER2^+$ (3.5%) breast cancer showed GFRA1 protein expression (Fig. 1E). In addition, GFRA1 staining was compared in 14 matched primary and metastatic tumors, with 6 pairs showing similar expression (IHC2+/3+) in both, 3 staining only in the primary tumor and 5 staining only in the metastasis. We have also tested for GFRA1 expression in human normal tissue panel by IHC analysis. GFRA1 is weakly (IHC1+) expressed in normal breast (2/3), kidney (2/3), salivary gland (1/3) and peripheral nerve tissues (3/3). No significant expression is observed in other normal tissues.

Development of anti-human GFRA1 antibodies

Mature GFRA1 is a cell-surface protein consisting of 429 amino acids with a glycosylphosphatidylinositol (GPI)-anchor as a membrane attachment. To generate anti- GFRA1 antibodies, mice were immunized with recombinant GFRA1-Fc fusion protein consisting of GFRA1 extracellular domain (ECD, aa 19-429). Sixteen FACS positive antibodies were identified on GFRA1 transfected cell lines and their binding to GFRA1-ECD was confirmed by BIAcore analysis with *Kd* values in the range of 0.5 to 10 nmol/L (Supplementary Table S1), with 6D3 and 7C9 showing the highest affinities. All these antibodies were specific to GFRA1 and did not cross-react with its closest homolog, GFRA2 (GFRA2 showed 46.5% identity to GFRA1) when tested by ELISA analysis (Supplementary Fig. S2).

Anti-GFRA1 antibody exhibits effective cellular internalization

An ideal ADC binds to its corresponding antigen on the tumor cell-surface and undergoes internalization followed by lysosomal degradation and the antigen–ADC complex, liberating free cytotoxic drug (15, 16). Internalization properties are often driven by the tumor antigen and GPI-lipid anchored proteins are typically endocytosed via a clathrin-independent lipid raft (CLIC/GLEEC) pathway (17). Because GFRA1 is GPI-anchored, we used immunofluorescence to evaluate the uptake of the anti-GFRA1 antibody 6D3 upon binding to GFRA1 expressing HEK293 cells. We observed an excellent cell surface staining of GFRA1 at 0 hours time, whereas after 2 hours we noted the co-localization (yellow) of GFRA1 staining (green) with late endosomal/lysosomal marker (red, LAMP2). Complete co-localization of anti-GFRA1 was observed with LAMP2 by the 16 hours time point (Fig. 2A), indicating effective lysosomal delivery of this antibody, supporting its conjugation to cytotoxic payload via a cleavable linker to create an ADC.

Anti-GFRA1 antibodies do not inhibit the GDNF/RET signaling pathway

GFRA1 in complex with its ligand GDNF binds RET tyrosine kinase and contributes to downstream MAPK signaling (18). Mice lacking GFRA1 are shown to exhibit similar phenotypes as RET or GDNF knockout mice, namely deficits in kidney, enteric nervous system, spinal motor and sensory neurons (19). Thus, anti-GFRA1 antibodies that do not interfere in normal cellular functions of the GDNF/RET signaling pathway would be ideal candidates for ADC therapeutic development. We tested the two highest affinity anti-GFRA1 antibodies (mu-6D3 and mu-7C9) for their ability to interfere with GDNF-induced RET signaling in MCF7 cells by monitoring

Published OnlineFirst December 27, 2017; DOI: 10.1158/1535-7163.MCT-17-0813

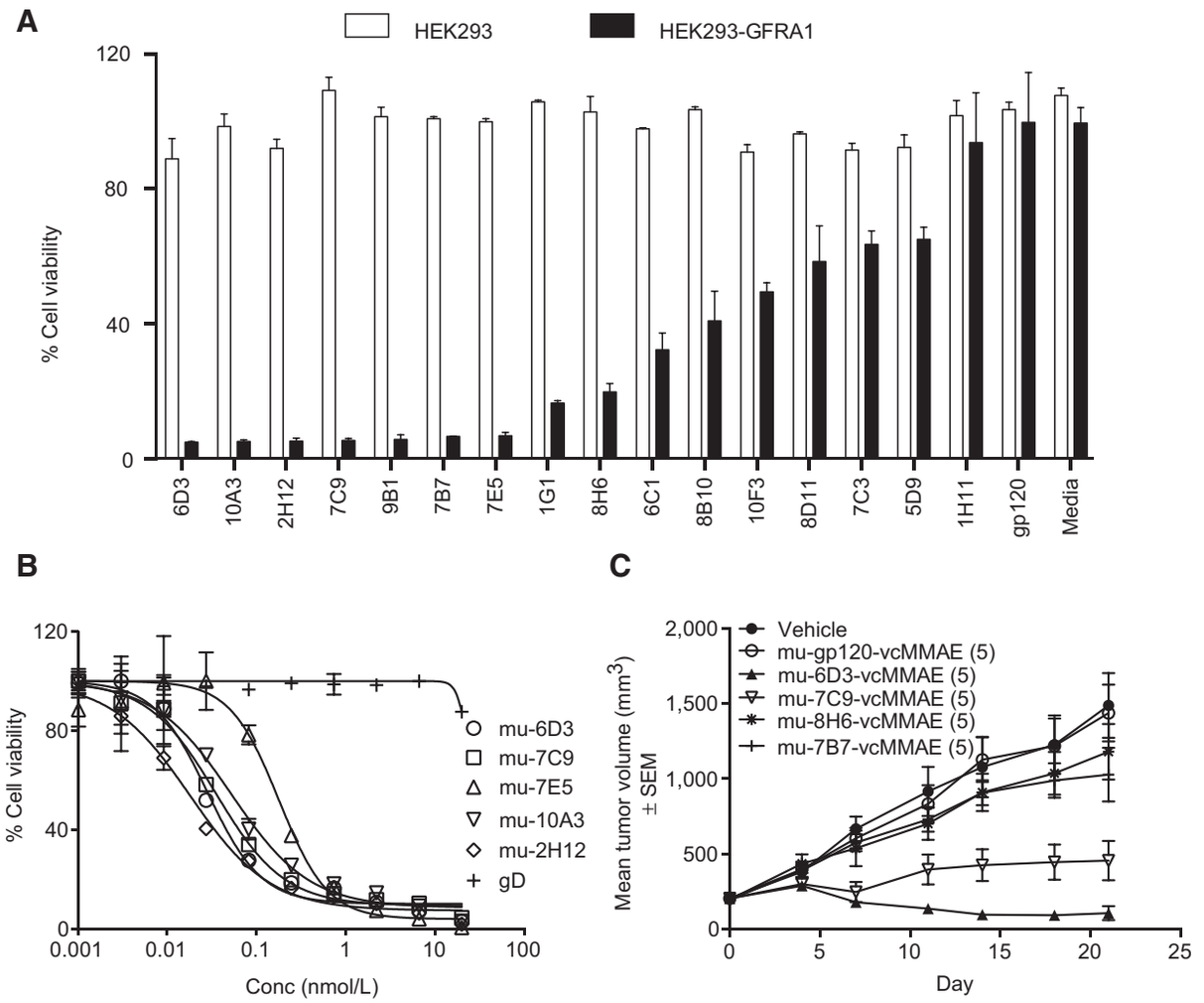

Figure 3.

Anti-GFRA1 ADCs display target-dependent *in vitro* and *in vivo* potency. **A,** Panel of FACS-positive anti-GFRA1 antibodies were conjugated with vcMMAE linker-payload and incubated for 3 days with HEK293 or HEK293-GFRA1 (IHC score for GFRA1 at 2+/3+) cells at 2 μg/mL. **B,** Dose response of most potent subset of anti-GFRA1 ADCs on HEK293-GFRA1 cells. **C,** *In vivo* efficacy of anti-GFRA1 ADCs. On the day of randomization, mice were given a single, intravenous dose of either a control (non-binding) ADC (anti–gp120-vcMMAE) or anti–GFRA1-ADC (anti–GFRA1-vcMMAE) at the doses indicated in parentheses (in mg/kg). Murine anti-GFRA1 ADCs were tested in the MCF7-neo/HER2 tumor model (IHC score for GFRA1 at 1+/2+).

MAPK or ERK phosphorylation. As shown in Fig. 2B, these antibodies had no effect on signaling at 1 μg/mL, thus GDNF/GFRA1 activity is retained, supporting selection of such antibodies for use as ADCs.

GFRA1 ADCs displayed target-dependent cell killing *in vitro* and *in vivo*

Hybridoma-based antibody development efforts resulted in 16 FACS-positive antibodies. Affinity screening by BIAcore or $FACS^+$ analysis is one of the methods routinely used to select the lead antibodies. However, such screens do not incorporate all properties desired of an antibody (such as internalization) for use as an ADC. Screening and selection of the lead antibodies based on ADC-mediated cell killing would be far superior, but would be labor intensive and cost ineffective at typical 10 to 20 mg scales. We therefore developed a 96-well format small-scale conjugation protocol (<1 mg ADC) to conjugate all 16 murine anti-GFRA1 antibodies with a cleavable linker-payload (vcMMAE) as described in Materials and Methods. All anti-GFRA1-vcMMAE ADCs and a control non-binding ADC (anti–gp120-vcMMAE) at 2 μg/mL or media alone (without any added ADC) were incubated with either HEK293 or HEK293-GFRA1 cells for 3-days and quantitated viable cells using the CellTiter-Glo assay. At this ADC concentration, the non-binding control ADC (gp120 ADC) showed minimal effect on either HEK293 or HEK293-GFRA1 cells, whereas select GFRA1-ADCs showed target-specific cell killing (Fig. 3A). The best anti-GFRA1 ADCs (6D3, 7C9, 7E5, 10A3, and 2H12) were further characterized at various ADC concentrations on HEK293- GFRA1 cells, all GFRA1 ADCs showing target dependent killing, with similar IC_{50}s around 0.03 nmol/L, although 7E5 was slightly less effective at 0.18 nmol/L (Fig. 3B).

Published OnlineFirst December 27, 2017; DOI: 10.1158/1535-7163.MCT-17-0813

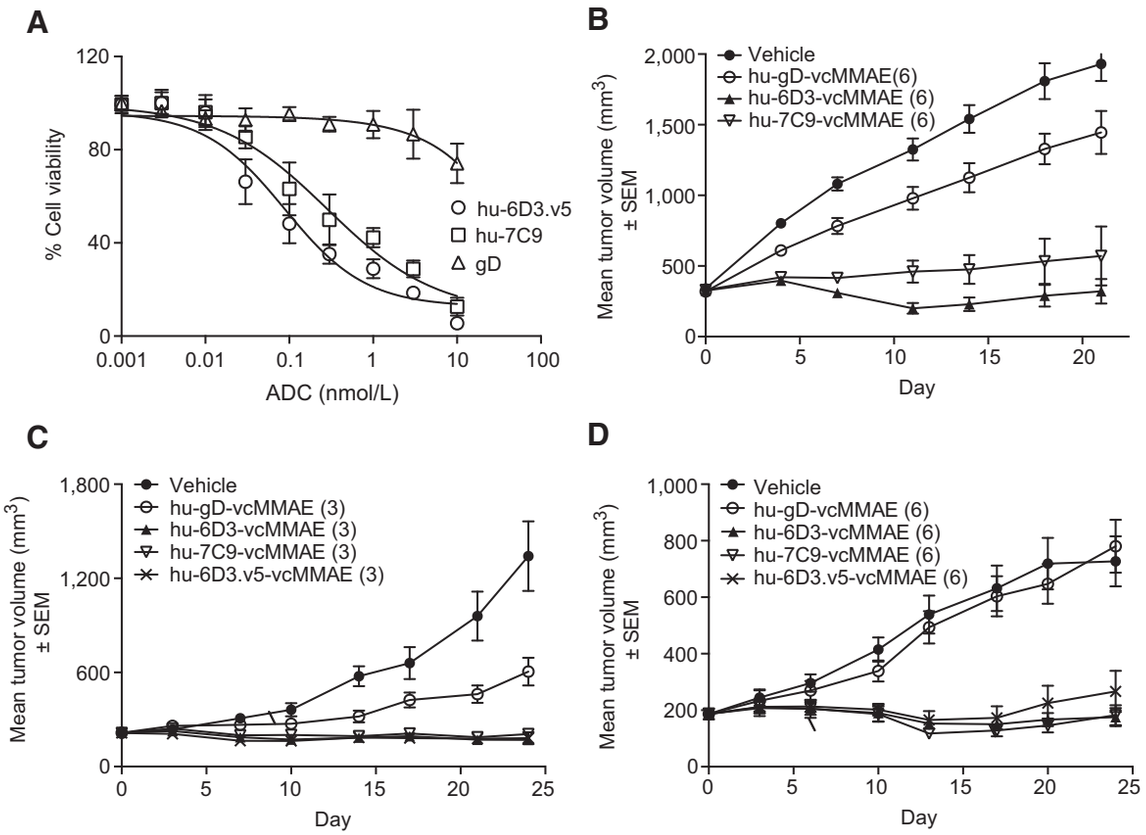

Figure 4.

Humanized anti-GFRA1 ADCs display robust *in vitro* potency and *in vivo* efficacy in tumor xenograft models that matched for GFRA1 expression levels to those of breast cancer patients. **A,** Potency of lead humanized anti-GFRA1 ADCs (hu-6D3.v5 and hu-7C9) on MCF7-neo/HER2 cell line. Lead humanized anti-GFRA1 ADCs were tested in the MCF7-neo/HER2 (**B**), KPL-1 (**C**), and MCF7 (**D**) xenograft models. Anti–gD-vcMMAE was used as a non-binding ADC control. Dose of ADCs tested is stated in parentheses as mg/kg. All three tumor models have IHC score for GFRA1 at 1+/2+.

IHC score of 2+/3+ levels were observed in 75% of GFRA1 +ve luminal A breast cancer tissues, while remaining 25% were at 1+ levels. We have screened and identified MCF7-neo/HER2, MCF7 and KPL-1 as clinically relevant cell line models as they express GFRA1 at low to moderate levels (IHC score of 1+/2+). To determine the therapeutic potential of anti-GFRA1 ADCs, we evaluated their activity against xenografts of MCF7-neo/HER2 cells *in vivo*. Administration of a single, 5 mg/kg dose of four different murine anti-GFRA1 ADCs exhibited varying degrees of efficacy against MCF7-neo/HER2 tumors (Fig. 3C). There was no evidence of antitumor activity with either mu-7B7 ADC or mu-8H6 ADC, whereas mu-7C9 ADC caused tumor stasis (3 PR) and mu-6D3 ADC resulted in tumor regression (5 PR and 2 CR; Fig. 3C).

Development and characterization of humanized anti-GFRA1 ADCs

On the basis of the *in vitro* and *in vivo* ADC potency and antibody affinity, 6D3 and 7C9 antibodies were selected as lead antibody candidates for humanization, as described in Materials and Methods. An unpaired cysteine residue in the variable region of the 6D3 antibody that might interfere with linker-payload conjugation was mutated to serine or alanine residue, but resulted in a 5-fold decrease in the affinity. Affinity maturation identified a lead hu-6D3.v5 variant. Both hu-6D3.v5 and hu-7C9 showed binding affinities on GFRA1 expressing cells similar to those of their chimeras (mouse variable, human constant; Supplementary Table S1) and their corresponding ADCs showed greater *in vitro* potency on MCF7-neo/HER2 cells than a non-targeting anti-gD ADC (Fig. 4A).

Administration of a single, 6 mg/kg dose of either hu-7C9 ADC or hu-6D3 and hu- 6D3.v5 ADC (see Supplementary Table S2 for ADC bioanalytics) resulted in MCF7-neo/HER2 tumor stasis (2 PR) or tumor regression (4 PR), respectively (Fig. 4B), which is similar to the response observed with their murine ADC counterparts. In addition, we also evaluated their activity against the KPL-1 and MCF7 breast cancer models, both of which express GFRA1 at low to moderate levels (IHC score of 1+ or 2+) like MCF7-neo/HER2. In the KPL-1 model, administration of a single, 3 mg/kg dose of hu-6D3.v5 ADC, hu-7C9 ADC, or hu-6D3 ADC resulted in substantial, yet similar, anti-tumor activity, resulting in tumor growth inhibition with PRs in both the hu-6D3.v5 ADC

Published OnlineFirst December 27, 2017; DOI: 10.1158/1535-7163.MCT-17-0813

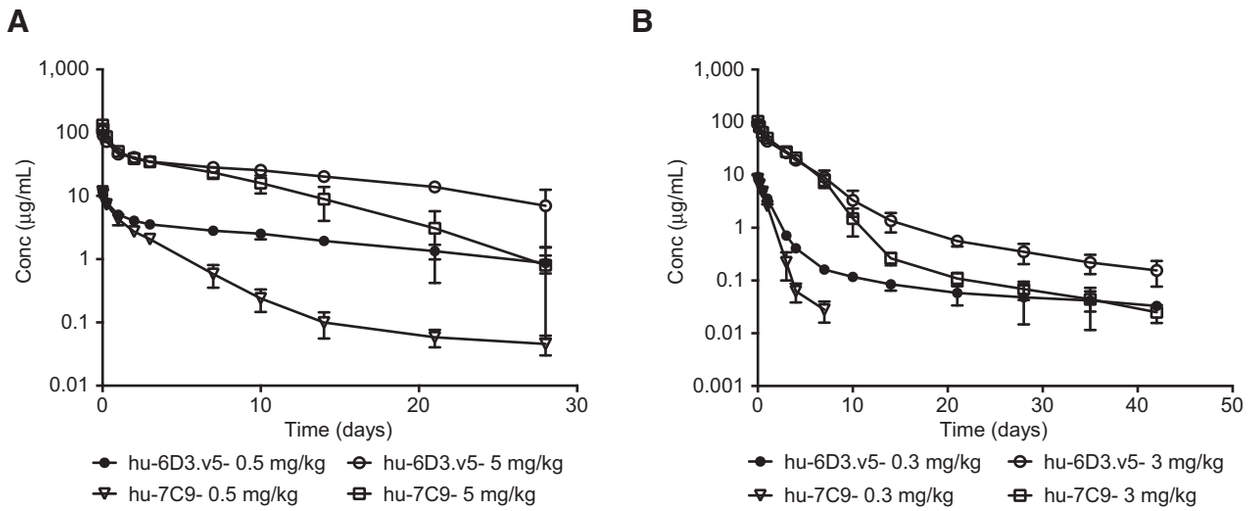

Figure 5.

Pharmacokinetics of humanized anti-GFRA1 antibodies in rats and non-human primates. **A,** Group mean (±SD) serum antibody concentrations following single intravenous administration of 0.5 mg/kg and 5 mg/kg hu-6D3.v5 or hu-7C9 in Sprague Dawley rats. **B,** Group mean (±SD) serum antibody concentrations following single intravenous administration of 0.3 mg/kg and 3 mg/kg hu-6D3.v5 or hu-7C9 in cynomolgus monkeys.

and hu-6D3 ADC groups (3 PR and 1 PR, respectively; Fig. 4C). In the MCF7 model, substantial tumor growth inhibition was also observed after a single, 6 mg/kg dose of hu-6D3.v5 ADC, hu-7C9 ADC, or hu-6D3 ADC with 3, 3 and 2 PRs, respectively; Fig. 4D).

ADC exposure, characterized by both total antibody and conjugated antibody (20), was estimated in MCF7-neo/HER2 and KPL-1 xenograft models. Similar to anti-GFRA1 antibodies PK in rats and cynomolgus monkeys (Fig. 5), hu-7C9 ADC cleared faster than either hu-6D3 ADC or hu-6D3.v5 ADC in mice (Supplementary Fig. S3). This exposure difference might have minimal effect on the anti-tumor activity in MCF7-neo/HER2 xenograft model (Fig. 4B) but had no effect on the efficacy in KPL-1 (Fig. 4C). Also, as expected for an ADC PK (15), conjugated antibody cleared faster than total antibody following ADC dose in mice (Supplementary Fig. S3).

Lead anti-GFRA1 antibodies cross-react with rodent and non-human primate GFRA1 protein

To properly assess the safety and pharmacologic properties of an ADC, the antibody should cross-react with the orthologous protein expressed by the test species. Mouse, rat, and cynomolgus monkey GFRA1 ortholog proteins are 92.94%, 88.88%, and 98.49% identical to human GFRA1, respectively. We cloned and expressed the full-length proteins of these species in HEK293 cells and tested binding of anti-GFRA1 antibody by FACS analysis. All GFRA1 proteins from four different species showed overlapping FACS titration curves upon binding to the hu-6D3.v5 and hu-7C9 (Supplementary Fig. S4A and S4B) and they all had a similar apparent *Kd* value of 1 nmol/L.

Pharmacokinetic characterization of humanized anti-GFRA1 antibodies in rats and cynomolgus monkeys

The PK profiles of hu-6D3.v5 and hu-7C9 following a single intravenous bolus dose at 0.5 or 5 mg/kg in female Sprague Dawley rats are shown in s 5A and PK parameters are summarized in Table 1. For the PK of hu-6D3.v5, as the dose increased from 0.5 to 5 mg/kg, the area under the serum concentration−time curve extrapolated to infinity (AUCinf) increased dose proportionally and clearance (CL) did not change with increasing doses, from 6.43 ± 1.23 mL/day/kg at 0.5 mg/kg dose to 6.55 ± 1.17 mL/d/kg at 5 mg/kg dose. The volume of distribution at steady-state (Vss) was also similar between the two dose levels, suggesting that the PK of hu-6D3.v5 was linear in this dose range of 0.5 to 5 mg/kg in rats. By contrast, the AUCinf)= of hu-7C9 increased more than dose proportionally and clearance (CL) decreased with increasing doses, from 24.7 ± 5.30 mL/d/kg at 0.5 mg/kg to 11.7 ± 2.64 mL/d/kg at 5 mg/kg, suggesting that the PK of hu-7C9 was nonlinear at this dose range.

The PK profiles of hu-6D3.v5 and hu-7C9 following a single intravenous bolus dose at 0.3 or 3 mg/kg in cynomolgus monkeys

Table 1. Pharmacokinetic characterization of anti-GFRA1 ADCs in rats and cynomolgus monkeys

	Rat				Cynomolgus monkey			
	hu-6D3.v5		hu-7C9		hu-6D3.v5		hu-7C9	
Parameters	0.5 mg/kg	5 mg/kg	0.5 mg/kg	5 mg/kg	0.3 mg/kg	3 mg/kg	0.3 mg/kg	3 mg/kg
C_{max} (mg/mL)	11.8 ± 1.5	107 ± 8.4	11.8 ± 0.7	132 ± 13.0	9.30 ± 1.1	93.9 ± 6.9	8.32 ± 0.7	104 ± 4.1
AUC_{inf} (day ·mg/mL)	79.8 ± 13.4	778 ± 127	20.9 ± 4.1	445 ± 108	13.9 ± 3.06	240 ± 46.1	8.08 ± 0.8	235 ± 26.3
CL (mL/day/kg)	6.4 ± 1.2	6.5 ± 1.2	24.7 ± 5.3	11.7 ± 2.6	22.4 ± 5.1	12.8 ± 2.1	37.4 ± 3.7	12.9 ± 1.5
Vss (mL/kg)	102 ± 7.6	101 ± 26.4	83.0 ± 5.3	71.8 ± 6.7	107 ± 30.5	58.4 ± 4.76	29.2 ± 1.1	36.3 ± 2.1
$t_{1/2}$ (day)	11.6 ± 2.4	11.2 ± 5.3	NR	NR	NR	NR	NR	NR

Abbreviations: AUC_{inf}, area under the serum concentration-time curve extrapolated to infinity; CL, clearance; C_{max}, observed maximum serum concentration; NR, not reported, due to a nonlinear pharmacokinetic profile; $t_{1/2,}$ half-life of the elimination phase; V_{ss}, volume of distribution at steady state.

Published OnlineFirst December 27, 2017; DOI: 10.1158/1535-7163.MCT-17-0813

are shown in Fig. 5B and PK parameters are summarized in Table 1. The PK of both hu-6D3.v5 and hu-7C9, as the dose increased from 0.3 to 3 mg/kg, area under the AUCinf increased more than dose proportionally and clearance (CL) decreased with increasing doses, from 22.4 ± 5.15 mL/d/kg at 0.3 mg/kg to 12.8 ± 2.13 mL/d/kg at 3 mg/kg for hu-6D3.v5; and from 37.4 ± 3.71 mL/d/kg at 0.3 mg/kg to 12.9 ± 1.46 mL/day/kg at 3 mg/kg for hu-7C9. Thus, the PK of both antibodies is nonlinear in the dose range of 0.3 to 3 mg/kg in cynomolgus monkeys, with hu-7C9 being more non-linear than hu-6D3.v5. Thus, in both species, hu-6D3.v5 exhibited lower clearance and was therefore chosen as the lead antibody.

Anti-GFRA1 ADC safety assessment in rats

In light of the weak to moderate expression of GFRA1 observed in peripheral nervous tissues, we set out to test safety of anti–GFRA1-vc-MMAE ADC in rats. Because the lead anti-GFRA1 antibodies were cross-reactive to rat GFRA1, evaluation of GFRA1 ADC's antigen-dependent toxicity was conducted in Sprague Dawley rats. Trastuzumab-vcMMAE (HER2 ADC) was used as a control to monitor antigen-independent ADC toxicity, as trastuzumab does not cross-react with rodent species (21). Rats were dosed intravenously on day 1 and 8 with GFRA1 ADC at 10 or 20 mg/kg, and HER2 ADC at 20 mg/kg. In general, GFRA1 ADC and HER2 ADC were well tolerated up to 20 mg/kg in rats. There were no mortalities, clinical signs or body weight changes observed throughout the study period in either ADC group. In addition, there were no clear GFRA1 ADC or HER2 ADC-related neurobehavioral effects noted in the functional observation battery (FOB) or motor activity parameters. The main toxicity observed was in the bone marrow, and was characterized by decreases in reticulocytes, red blood cell counts, hemoglobin, hematocrit and absolute neutrophil counts (Fig. 6A and B); hematologic changes correlated with sternal and femoral bone marrow hypocellularity. There was a slight increase in the severity of neutrophil depletion in the 20 mg/kg GFRA1 ADC group compared with HER2 ADC, but the remaining toxicologic parameters were similar between test articles. Additional changes in histopathology included decreased lymphoid cellularity in the thymus and mandibular lymph nodes. Clinical chemistry findings were consistent with inflammation and liver injury observed in the 20 mg/kg groups, as evidenced by increases in alanine aminotransferase (ALT), aspartate aminotransferase (AST), gamma glutamyltransferase (GGT), and bilirubin (Fig. 6C). However, there was no liver injury observed microscopically. There were no macroscopic and microscopic abnormalities observed in the central nervous and peripheral nervous tissues.

Discussion

The design and development of an ADC relies on four key features: (i) A cell-surface protein target that is minimally expressed in normal tissues and abundantly expressed in tumor tissues; (ii) A stable linker-payload in the plasma to minimize off-target toxicity due to linker failure; (iii) Internalization of the target protein/antibody complex to effectively deliver payload into target protein expressing cancer cells; (iv) A lead antibody with optimal PK properties for its effective tumor targeting (16). We applied these four criteria to select and develop an anti-GFRA1 ADC, hu-6D3.v5-vcMMAE, for targeting of luminal A (hormone receptor-positive) breast cancer.

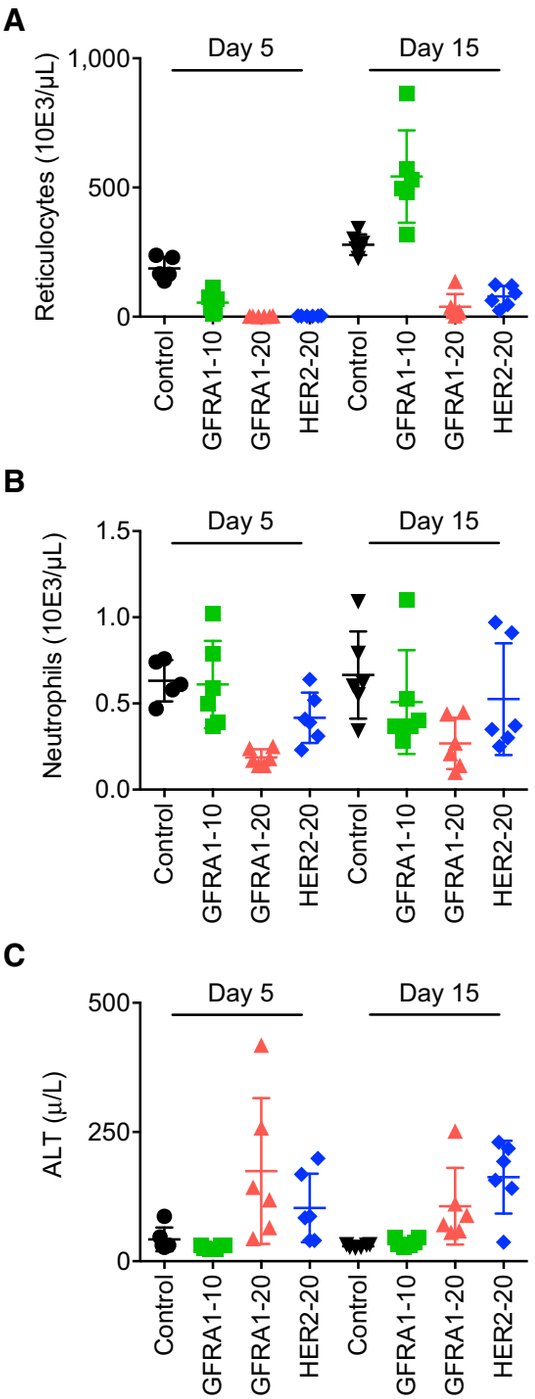

Figure 6.
Safety assessment of anti-GFRA1 ADC in Sprague-Dawley rats. **A,** Marked decreased absolute reticulocyte count on day 5 in animals administered 10 or 20 mg/kg GFRA1 ADC, or 20 mg/kg HER2 (trastuzumab, Tmab) ADC. On day 15, rebound reticulocyte count was evident at 10 mg/kg, whereas decreased reticulocyte count was persistent for the 20 mg/kg animals, or 20 mg/kg HER2 ADC. **B,** Mild decreased absolute neutrophil counts on days 5 and 15 in animals administered 20 mg/kg GFRA1 ADC. **C,** Mild to moderate increase in alanine aminotransferase (ALT) level on days 5 and 15 in animals administered 20 mg/kg GFRA1 ADC, or 20 mg/kg HER2 ADC.

Published OnlineFirst December 27, 2017; DOI: 10.1158/1535-7163.MCT-17-0813

We corroborated earlier reports (5) of GFRA1 overexpression in luminal A breast cancers, finding 70% of positive samples in which 75% were 2+/3+. The GFRA1 transcript levels correlates well with protein expression in a luminal A breast cancer tissues, suggesting that a high-throughput RNA-based diagnostic assay might suffice for patient selection instead of a IHC. RET, a receptor in GDNF-signaling is also known to be overexpressed in the breast cancer tissues (5, 22), but we found it inferior to GFRA1 at both the mRNA and protein level, with only 6/29 (20%) samples expressing RET at 2+/3+ in line with previous reports (20). Our IHC analysis further confirmed that RET is overexpressed with IHC score of 2+/3+ only in 20% (6 of 29) patients, while 28% (8 of 29) patients showed IHC score 1+ and 52% (15 of 29) luminal A breast cancer patients showed no expression. B7H4 and Ly6E protein targets were also reported to be expressed in breast cancer tissues and both these targets showed IHC score of 2+/3+ at 37% and 61% expression, respectively, in hormone receptor-positive breast cancer patients (23, 24). On the basis of the protein expression criteria as described above, GFRA1 is therefore a potentially superior ADC target for the treatment of luminal A breast cancer.

We chose the cathepsin cleavable val-cit-MMAE linker-drug to conjugate to the anti-GFRA1 antibody for a few reasons. The val-cit-MMAE linker-payload was shown to be stable in plasma (12) and proven to be effective with several ADC targets (as summarized in refs. 15, 25). In addition, MMAE, a tubulin binder, preferentially kills proliferating cells, whereas DNA damaging payloads, such as duocarmycins, calicheamicins or pyrrolobenzodiezepines, are known to kill both proliferating and non-proliferating cells. The vcMMAE linker-payload also has not exhibited any target-dependent toxicity with most ADC targets (15). With respect to this, the IHC analysis in normal tissues revealed that GFRA1 protein is expressed in peripheral nervous tissues at weak levels (IHC score of 1+). Therefore, selection of MMAE as a payload may be a safer option for this ADC target.

Internalization of an ADC is a very important feature and is primarily governed by its cell-surface target antigen (16). Despite being GPI-anchored the lead anti-GFRA1 antibody internalized well and mediated target-specific ADC cell killing in GFRA1-expressing cells even after humanization. In addition, the lead humanized anti-GFRA1 ADC showed a target-dependent therapeutic activity in three different GFRA1 expressing tumor xenograft models with 1+ or 2+ GFRA1 expression similar to that seen in breast cancer patients. Importantly, we did not observe any adverse neurologic safety findings with anti- GFRA1-vc-MMAE ADC, despite expression of the target in peripheral nerves. Furthermore, the lead 6D3 antibody does not interfere with the GDNF/RET signaling pathway, avoiding potential safety issues of blocking normal tissue growth and development.

In summary, hu-6D3.v5 anti-GFRA1 ADC is an excellent ADC for luminal A (hormone receptor-positive) breast cancer, which accounts for over 70% of breast cancer patients and has potential utility as a targeted therapy for many relapsed luminal A breast cancer patients.

Disclosure of Potential Conflicts of Interest

No potential conflicts of interest were disclosed by the authors.

Authors' Contributions

Conception and design: S. Bhakta, M.M. Schutten, D. Li, D. Sampath, M.S. Dennis, P. Polakis, J.R. Junutula

Development of methodology: S. Bhakta, K.A. Poon, A. Fourie-O'Donohue, K.R. Kozak, H. Raab, J.R. Junutula

Acquisition of data (provided animals, acquired and managed patients, provided facilities, etc.): L.M. Crocker, Y. Chen, M. Hazen, C. Kuijl, R. Ohri, K.A. Poon, M.A.T. Go, E. Cheng, R. Firestein, A. Fourie-O'Donohue, D. Sampath

Analysis and interpretation of data (e.g., statistical analysis, biostatistics, computational analysis): L.M. Crocker, M.M. Schutten, D. Li, C. Kuijl, R. Ohri, F. Zhong, K.A. Poon, R. Piskol, R. Firestein, A. Fourie-O'Donohue, K.R. Kozak, D. Sampath, J.R. Junutula

Writing, review, and/or revision of the manuscript: S. Bhakta, L.M. Crocker, M. Hazen, M.M. Schutten, D. Li, R. Ohri, F. Zhong, R. Piskol, A. Fourie-O'Donohue, K.R. Kozak, J.-A. Hongo, D. Sampath, R.H. Scheller, P. Polakis, J.R. Junutula

Administrative, technical, or material support (i.e., reporting or organizing data, constructing databases): S. Bhakta, L.M. Crocker, D. Li, J.-A. Hongo, M.S. Dennis, R.H. Scheller, J.R. Junutula

Study supervision: K.A. Poon, D. Sampath, M.S. Dennis, J.R. Junutula

Acknowledgments

We thank our Genentech, Inc. colleagues: early-stage cell culture and protein chemistry departments for their help with large-scale production of anti-GFRA1 antibodies; oligonucleotide synthesis facility for generating needed DNA primers for molecular cloning, gCell and *in vivo* cell culture core facility and dosing technicians for support of *in vivo* efficacy studies; Linda Ringall and IHC core facility for IHC analyses; Susan D. Spencer for her assistance with project management and ADC material supply; Jyoti Asundi, Dr. Andrew Polson and Dr. Suzie Scales for critical review of the article.

The costs of publication of this article were defrayed in part by the payment of page charges. This article must therefore be hereby marked *advertisement* in accordance with 18 U.S.C. Section 1734 solely to indicate this fact.

Received August 25, 2017; revised November 17, 2017; accepted December 18, 2017; published OnlineFirst December 27, 2017.

References

1. Howlader N, Noone AM, Krapcho M, Miller D, Bishop K, Kosary CL, et al. SEER Cancer Statistics Review 2016; 2016:1975–2014. Available from: https://seer.cancer.gov/csr/1975_2014/
2. American Cancer Society. Breast Cancer Facts & Figures 2015–2016. Atlanta, GA: American Cancer Society.
3. Mendes D, Alves C, Afonso N, Cardoso F, Passos-Coelho JL, Costa L, et al. The benefit of HER2-targeted therapies on overall survival of patients with metastatic HER2-positive breast cancer – a systematic review. Breast Cancer Res 2015;17:140.
4. Morandi A, Martin LA, Gao Q, Pancholi S, Mackay A, Robertson D, et al. GDNF-RET signaling in ER-positive breast cancers is a key determinant of response and resistance to aromatase inhibitors. Cancer Res 2013;73:3783–95.
5. Esseghir S, Todd SK, Hunt T, Poulsom R, Plaza-Menacho I, Reis-Filho JS, et al. A role for glial cell derived neurotrophic factor induced expression by inflammatory cytokines and RET/GFR alpha 1 receptor up-regulation in breast cancer. Cancer Res 2007;67:11732–41.
6. Junutula JR, Gerber HP. Next-generation antibody-drug conjugates (ADCs) for cancer therapy. ACS Med Chem Lett 2016;7:972–3.
7. Beck A, Goetsch L, Dumontet C, Corvaia N. Strategies and challenges for the next generation of antibody-drug conjugates. Nat Rev Drug Discov 2017;16:315–37.
8. Wu TD, Nacu S. Fast and SNP-tolerant detection of complex variants and splicing in short reads. Bioinformatics 2010;26:873–81.
9. Law CW, Chen Y, Shi W, Smyth GK. voom: precision weights unlock linear model analysis tools for RNA-seq read counts. Genome Biol 2014;15:R29.
10. Ritchie ME, Phipson B, Wu D, Hu Y, Law CW, Shi W. limma powers differential expression analyses for RNA-sequencing and microarray studies. Nucleic Acids Res 2015;43:e47.

Published OnlineFirst December 27, 2017; DOI: 10.1158/1535-7163.MCT-17-0813

11. Srinivasan K, Friedman BA, Larson JL, Lauffer BE, Goldstein LD, Appling LL, et al. Untangling the brain's neuroinflammatory and neurodegenerative transcriptional responses. Nat Commun 2016;7:11295.
12. Doronina SO, Toki BE, Torgov MY, Mendelsohn BA, Cerveny CG, Chace DF, et al. Development of potent monoclonal antibody auristatin conjugates for cancer therapy. Nat Biotechnol 2003;21:778–84.
13. Lee CV, Koenig P, Fuh G. A two-in-one antibody engineered from a humanized interleukin 4 antibody through mutation in heavy chain complementarity- determining regions. MAbs 2014;6: 622–7.
14. Chen Y, Wiesmann C, Fuh G, Li B, Christinger HW, McKay P, et al. Selection and analysis of an optimized anti-VEGF antibody: crystal structure of an affinity-matured Fab in complex with antigen. J Mol Biol 1999;293: 865–81.
15. Polakis P. Antibody drug conjugates for cancer therapy. Pharmacol Rev 2016;68:3–19.
16. Panowski S, Bhakta S, Raab H, Polakis P, Junutula JR. Site-specific antibody drug conjugates for cancer therapy. MAbs 2014;6:34–45.
17. Mayor S, Parton RG, Donaldson JG. Clathrin-independent pathways of endocytosis. Cold Spring Harb Perspect Biol 2014;6:1–20.
18. Mulligan LM. RET revisited: expanding the oncogenic portfolio. Nat Rev Cancer 2014;14:173–86.
19. Enomoto H, Araki T, Jackman A, Heuckeroth RO, Snider WD, Johnson EM Jr, et al. GFR alpha1-deficient mice have deficits in the enteric nervous system and kidneys. Neuron 1998;21:317–24.
20. Kaur S, Xu K, Saad OM, Dere RC, Carrasco-Triguero M. Bioanalytical assay strategies for the development of antibody–drug conjugate biotherapeutics. Bioanalysis 2013;5:201–26.
21. Lewis Phillips GD, Li G, Dugger DL, Crocker LM, Parsons KL, Mai E, et al. Targeting HER2-positive breast cancer with trastuzumab-DM1, an antibody-cytotoxic drug conjugate. Cancer Res 2008;68:9280–90.
22. Nguyen M, Miyakawa S, Kato J, Mori T, Arai T, Armanini M, et al. Preclinical efficacy and safety assessment of an antibody-drug conjugate targeting the c-RET proto-oncogene for breast carcinoma. Clin Cancer Res 2015;21: 5552–62.
23. Leong SR, Liang WC, Wu Y, Crocker L, Cheng E, Sampath D, et al. An anti-B7-H4 antibody-drug conjugate for the treatment of breast cancer. Mol Pharm 2015;12:1717–29.
24. Asundi J, Crocker L, Tremayne J, Chang P, Sakanaka C, Tanguay J, et al. An antibody-drug conjugate directed against lymphocyte antigen 6 complex, Locus E (LY6E) provides robust tumor killing in a wide range of solid tumor malignancies. Clin Cancer Res 2015;21:3252–62.
25. Sievers EL, Senter PD. Antibody-drug conjugates in cancer therapy. Annu Rev Med 2013;64:15–29.

Molecular Cancer Therapeutics

Correction: An Anti-GDNF Family Receptor Alpha 1 (GFRA1) Antibody–Drug Conjugate for the Treatment of Hormone Receptor–Positive Breast Cancer

Sunil Bhakta, Lisa M. Crocker, Yvonne Chen, Meredith Hazen, Melissa M. Schutten, Dongwei Li, Coenraad Kuijl, Rachana Ohri, Fiona Zhong, Kirsten A. Poon, Mary Ann T. Go, Eric Cheng, Robert Piskol, Ron Firestein, Aimee Fourie-O'Donohue, Katherine R. Kozak, Helga Raab, Jo-Anne Hongo, Deepak Sampath, Mark S. Dennis, Richard H. Scheller, Paul Polakis, and Jagath R. Junutula

In the original version of this article (1), Fig. 4 was mistakenly replaced with a previous version when final materials were uploaded. Because of this error, Fig. 4A was a duplication of Fig. 3C. Figure 4 has been corrected to include the proper Fig. 4A. The error has been corrected in the latest online HTML and PDF versions of the article. The authors regret this error.

Reference

1. Bhakta S, Crocker LM, Chen Y, Hazen M, Schutten MM, Li D, et al. An Anti-GDNF family receptor alpha 1 (GFRA1) antibody–drug conjugate for the treatment of hormone receptor–positive breast cancer. Mol Cancer Ther 2018;17:638–49.

Published online November 1, 2019.
Mol Cancer Ther 2019;18:2182
doi: 10.1158/1535-7163.MCT-19-0749

AACR

Published OnlineFirst December 27, 2017; DOI: 10.1158/1535-7163.MCT-17-0813

AACR American Association for Cancer Research

Molecular Cancer Therapeutics

An Anti-GDNF Family Receptor Alpha 1 (GFRA1) Antibody–Drug Conjugate for the Treatment of Hormone Receptor–Positive Breast Cancer

Sunil Bhakta, Lisa M. Crocker, Yvonne Chen, et al.

Mol Cancer Ther 2018;17:638-649. Published OnlineFirst December 27, 2017.